American Mineralogist, Volume 81, pages 79–91, 1996

Formation of regularly interstratified serpentine-chlorite minerals by tetrahedral inversion in long-period serpentine polytypes

JILLIAN F. BANFIELD AND STURGES W. BAILEY*

Department of Geology and Geophysics, University of Wisconsin–Madison, 1215 West Dayton Street, Madison, Wisconsin 53706, U.S.A.

ABSTRACT

Serpentinite from Lancaster County, Pennsylvania, consists of a variety of fine-grained serpentine minerals, chlorite, randomly interstratified serpentine-chlorite, and a series of phases based on regular interstratification of serpentine and chlorite (S_xC_y, where x and y are integers). Within the resolution of the AEM technique, all layer silicates have the same Mg-rich, Al-rich, Cr-rich, and Fe-poor compositions. Regularly interstratified serpentine-chlorite minerals are frequently intimately intergrown with serpentines that have repeat distances identical to those of the regular interstratifications. Thus, dozyite (S_1C_1, $\beta = 90°$) is intimately associated with serpentine with three-layer octahedral order (I,I,II). Longer period polysomes (S_2C_1, S_1C_2, S_2C_2, S_1C_3, S_3C_2, and S_1C_4, all with $\beta = 90°$) are each accompanied by serpentines with equivalent c-axis periodicities. S_xC_y phases apparently form by selective growth of I*bb* chlorite units from I,II octahedral sequences in long-period serpentines. All microscopic structural evidence is consistent with the formation of regular interstratifications by tetrahedral inversion within existing serpentine. Atomic resolution images reveal that the tetrahedral sheet is displaced by $a/3$ where it inverts to form the 2:1 layer. A $\pm a/3$ shift is required for hydrogen bonding between OH of the newly formed brucite-like interlayer and O atoms of the 2:1 layer. The sense of the shift is determined by the strong interactions between the octahedral cations in the brucite-like interlayer and the Si in the 2:1 layer (direct superimposition, previously described as a type-a interaction, is strongly unfavorable). Distortion at the inversion point probably lengthens Si-O bonds in the next tetrahedra, facilitating relocation of Si on the other side of the basal O plane. Reversal of the octahedral slant in the 2:1 layer occurs because the $+a/3$ tetrahedral shift necessitates repositioning of O and OH coordinating octahedral cations, requiring movement of octahedral cations from type-II to type-I positions. Except in the 2:1 layers, the stacking and octahedral slants are inherited. The result is a series of regular interstratifications characterized by a single octahedral slant (specifically, I*bbb*,I) and $b/3$ stacking disorder. This analysis reveals the importance of cation-cation interactions in determining the relative stability of pairs of 1:1 layers and in controlling the detailed structures of layer silicates formed in solid-state serpentine-to-chlorite reactions. Because similar constraints apply to formation of serpentine from chlorite by direct structural modification, the common 1T lizardite polytype may be produced from both II*bb* and I*bb* chlorites.

INTRODUCTION

It is widely known that serpentine (S) transforms to chlorite (C) and vice versa (see chapters in Bailey 1988a) and that random serpentine-chlorite interstratifications occur (see summary by Reynolds 1988). The first data revealing that serpentine-to-chlorite and chlorite-to-serpentine reactions produce regularly and randomly interstratified serpentine-chlorite appeared recently (Bailey et al. 1993; Banfield et al. 1993; Xu and Veblen 1993). Previously, structures exhibiting long-range order (e.g., R > 1, Reynolds 1988) had been reported only for illite-smectite (Reynolds and Hower 1970) and glauconite-smectite (Thompson and Hower 1975). It is now clear that, in addition to the 1:1 serpentine-chlorite regular interstratification (S_1C_1, known as dozyite; Bailey et al. 1995), serpentine-rich phases, such as S_2C_1 and S_3C_1, and chlorite-rich phases, such as S_1C_2 and S_1C_3, also occur (Banfield et al. 1994; Bailey et al. 1995; Xu and Veblen, in preparation). Members of the S_xC_y polysomatic series have been identified from several additional localities (this paper; Veblen 1993 and 1994 personal communication), suggesting these minerals may be relatively common, at least as fine-grained constituents of complex serpentine-chlorite assemblages.

It is not known why long-period, regularly interstrati-

* Deceased November 30, 1994.

0003–004X/96/0102–0079$05.00

fied serpentine-chlorite minerals crystallize instead of discrete serpentine or chlorite or a random interstratification of these. Although the first examples involved rather Al-rich compositions (amesite; Bailey et al. 1993, 1995; Banfield et al. 1993, 1994), more recent data suggest the phenomenon is not limited to minerals with unusual characteristics. Other examples include Fe-rich (berthierene; Xu and Veblen 1993) and Mg- and Cr-rich serpentines (this paper).

Proposed origins for analogous regularly interstratified layer silicates [e.g., talc-chlorite (kulkeite), mica-smectite (rectorite), illite-smectite, biotite-vermiculite (hydrobiotite)] include dissolution-reprecipitation and transformation reactions involving varying degrees of structural inheritance. Microstructural data (specific groupings of layer types and antiphase relationships) strongly suggest that the $C \rightarrow S_xC_y$ and $S \rightarrow S_xC_y$ reactions occur by solid-state mechanisms (e.g., Banfield et al. 1993; Xu and Veblen 1993). Although complex members of this (and other) polysomatic series may form in an Ostwald sequence (e.g., a → ab → abb → abbb → . . .b), at least a subset of steps would require undoing previous structural changes. Dramatically different morphologies for coexisting regular interstratifications with different ratios of serpentine and chlorite argue against this process in the chlorite-to-serpentine reaction (Banfield et al. 1994).

In this paper, we present evidence for a new polytype of dozyite and reveal the detailed structures and microstructures of poorly known as well as previously undescribed regular interstratifications of serpentine and chlorite. We correlate the distribution and structure of regular interstratifications with the distribution and structure of specific serpentine polytypes. Thus, we consider the hypothesis that periodic chlorite development in serpentine is achieved by selective replacement of structurally and energetically distinct subunits within long-period serpentine precursors.

Experimental methods

Samples

Samples were from the Woods Chrome Mine in the State Line Serpentinite, Lower Britain Township, Lancaster County, Pennsylvania (Lapham 1958). Specimens were collected circa 1955 by R.C. Smith II from mine dumps (39°43′52″N, 76°06′20″W). The serpentine mineralogy and geology of the serpentine is described in detail in Banfield et al. (1995).

Sample preparation and transmission electron microscopy

Thin sections were prepared from strongly foliated samples, a centimeter wide by a few centimeters long. One section was cut normal to foliation defined by the silicate sheets and parallel to the lineation within the foliation, and a second was cut normal to both the foliation and lineation. Ten 3 mm diameter, 30 μm thick slices were removed from thin sections, mounted on copper support washers, and thinned to electron transparency by argon ion milling. Samples were carbon coated before examination in a 200 kV Philips CM20 UT high-resolution transmission electron microscope (HRTEM) with a point resolution of about 0.19 nm. Compositional analysis in the HRTEM was performed using a NORAN Ge detector and NORAN voyager software.

Serpentine-chlorite regular interstratifications were distinguished from serpentines using 00*l* periodicities in selected-area electron diffraction (SAED) patterns oriented to eliminate dynamical diffraction effects involving 20*l* rows. HRTEM images were interpreted to provide atomic structural and defect microstructural information by comparison with image simulations calculated using the proprietary EMS software (Stadelmann 1991).

Because the 00*l* intensities are sensitive to the sequence of structural units along [001], structures of regular interstratifications can be readily determined by comparing observed 00*l* intensities with those calculated for all possible serpentine and chlorite combinations with the appropriate *c*-axis repeats. Table 1 lists the atomic coordinates for one polytype of each S_xC_y phase with a *c*-axis periodicity up to 6.3 nm.[1] Calculations of SAED intensities employed wave-function outputs from image-simulation calculations generated using the EMS software. SAED patterns were recorded from the thinnest possible areas (<10 nm thick) to minimize dynamical diffraction effects. Calculations reveal that, in most cases, distinct intensity variations were not greatly obscured by dynamical diffraction in these thin regions.

Identification of standard serpentine polytypes followed Bailey (1988b). Nonstandard serpentine-polytype identification used procedures based on the positions and intensities of reflections in [010] and [100] patterns (Bailey and Banfield 1995). Results were reported in Banfield et al. (1995).

Results

Coexisting with long-period serpentine polytypes described in Banfield et al. (1995) are crystals consisting of random interstratifications of serpentine and chlorite, as well as phases that have SAED patterns that reveal a >1.4 nm regular periodicity in 00*l*. As discussed previously (e.g., Banfield et al. 1994; Bailey et al. 1995), this periodicity requires alternation along *c* of structurally distinct layers and cannot arise from stacking of a single structural unit (such as in the serpentine polytypes). Thus, when crystals are tilted so that only the 00*l* row is apparent, these phases can be readily distinguished from the long-period serpentine polytypes with 0.7 nm 00*l* (and >1.4 nm 20*l*) periodicities.

Regular interstratifications

d_{001} = 2.1 nm. The most common phase with a periodicity in 00*l* of >1.4 nm has d_{001} = 2.1 nm (Fig. 1).

[1] A copy of Table 1 can be obtained by ordering Document AM-96-606 from the Business Office, Mineralogical Society of America, 1015 Eighteenth Street NW, Suite 601, Washington, DC 20036. Please remit $5.00 in advance for the microfiche.

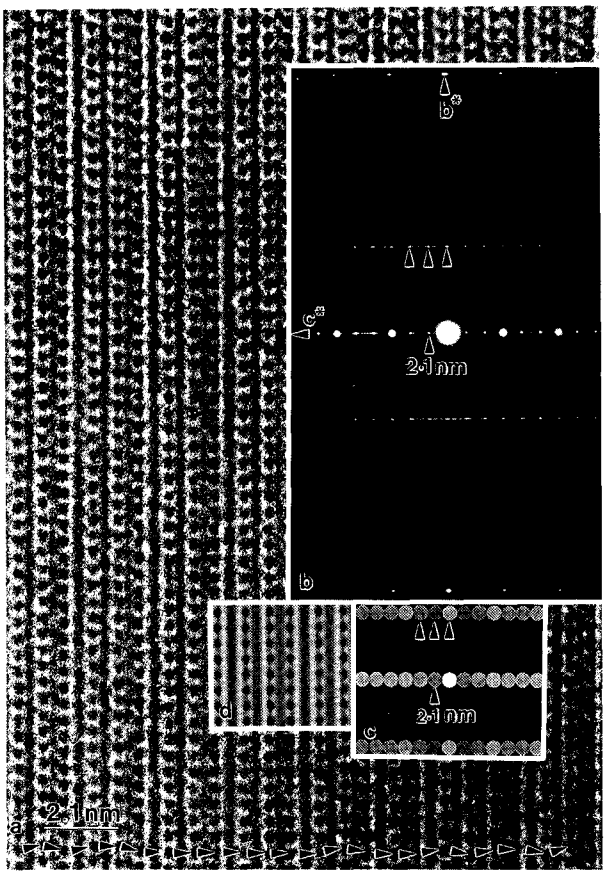

FIGURE 1. (**a**) HRTEM structural image down [100] illustrating an area of S_1C_1 (dozyite) with sufficient stacking regularity to produce spots (see arrows) in the $0kl$, $k \neq 3n$ rows in the SAED pattern shown in **b**. Arrows in **a** illustrate the sequence of $b/3$ displacements within the 2:1 layers and between the 2:1 and 1:1 layers. (**c**) Calculated SAED pattern for [100] dozyite, sample thickness of ~4 nm. (**d**) Calculated [100] image for dozyite, sample thickness ~4 nm, $C_s = 0.5$ mm, 200 kV. Note the correspondence between the observed and calculated images and diffraction patterns.

Details of the experimental image correspond very closely with those of the simulation (Fig. 1d), confirming that the darkest stripes represent brucite-like interlayers, the zipperlike strip corresponds to the 2:1 layer, and the one-half zipper to the 1:1 layer. Thus, the phase illustrated in Figure 1 is dozyite (S_1C_1), a regular 1:1 interstratification of serpentine and chlorite (Bailey et al. 1995; see Fig. 4 of that work for correspondence between structure and HRTEM image details).

An experimental SAED pattern (Fig. 1b) from S_1C_1 shows discrete $0kl$, $k \neq 3n$ reflections that are similar to those in the calculated SAED pattern (Fig. 1c), indicating some stacking order. The detailed stacking sequence can be extracted by examination of the positions of black spots corresponding to projected pairs of Si tetrahedra (see arrow sequence in Fig. 1a). Although some sub-sequences of black spots define straight lines, as in the image simulation calculated for the ideal structure (Fig. 1d), the stacking order is not perfect. This is also apparent from the streaking of the $k \neq 3n$ reflections (Fig. 1b). Although there is evidence for regular stacking in Figure 1, in almost all other layer-silicate crystals in the serpentinite samples the $0kl$, $k \neq 3n$ reflections are continuously streaked, indicating stacking disorder.

TABLE 2. Ideal atomic coordinates for dozyite I*bbb*,I

Atom	*x*	*y*	*z*
Mg	0	0	0
Mg	0.0000	0.3333	0.0000
O	0.3333	0	0.0493
O	0.3333	0.3333	0.0513
Si	0.3333	0.3333	0.1278
O	0.8333	0	0.1554
O	0.0833	0.2500	0.1554
O	0.6667	0	0.2865
O	0.6667	0.3333	0.2865
Mg	0.0000	0	0.3333
Mg	0.0000	0.3333	0.3333
O	0.3333	0	0.3801
O	0.3333	0.3333	0.3801
O	0.1667	0	0.5112
O	0.4167	0.2500	0.5112
Si	0.6667	0.3333	0.5388
O	0.6667	0	0.6173
O	0.6667	0.3333	0.6153
Mg	0.0000	0	0.6667
Mg	0.0000	0.3333	0.6667
O	0.3333	0	0.7135
O	0.3333	0.3333	0.7135
O	0.1667	0	0.8446
O	0.4167	0.2500	0.8446
Si	0.6667	0.3333	0.8722
O	0.6667	0	0.9507
O	0.6667	0.3333	0.9487

Note: Space group *Cm*, $a = 0.5323$, $b = 0.9214$, $c = 2.1381$ nm, and $\beta = 90.00°$.

The [010] SAED patterns have $\beta = 90°$, which distinguishes this polytype from that described in detail by Bailey et al. (1995). Calculated $20l$ intensities for a S_1C_1 phase with a I,I,I octahedral sequence have very weak $20l$, $l \neq 3n$. Intensities may be amplified by dynamical diffraction involving the $00l$ row. Although observed $20l$ electron diffraction intensities are consistent with either a I,I,II or I,I,I, octahedral cation sequence, examination of powder X-ray diffraction data suggests the structure is probably I*bbb*,I. Atomic coordinates for one structure are provided in Table 2.

The interface between dozyite (with a single extra serpentine layer) and serpentine is shown in Figure 2. Comparison of arrowed sequences defining $b/3$ stacking vectors in serpentine and dozyite indicates stacking order is the same in continuous layers, except across the point of tetrahedral inversion where 1:1 layers pass into 2:1 layers. Note that relative positions of tetrahedral pairs (black spots) in 1:1 layers bounding the 2:1 layers are not affected by displacements within the 2:1 layers, indicating the effect is localized.

Areas of defect-free dozyite are rare. Crystals frequently contain extra serpentine and, occasionally, extra chlorite units (Fig. 3a). Interfaces between regions with dif-

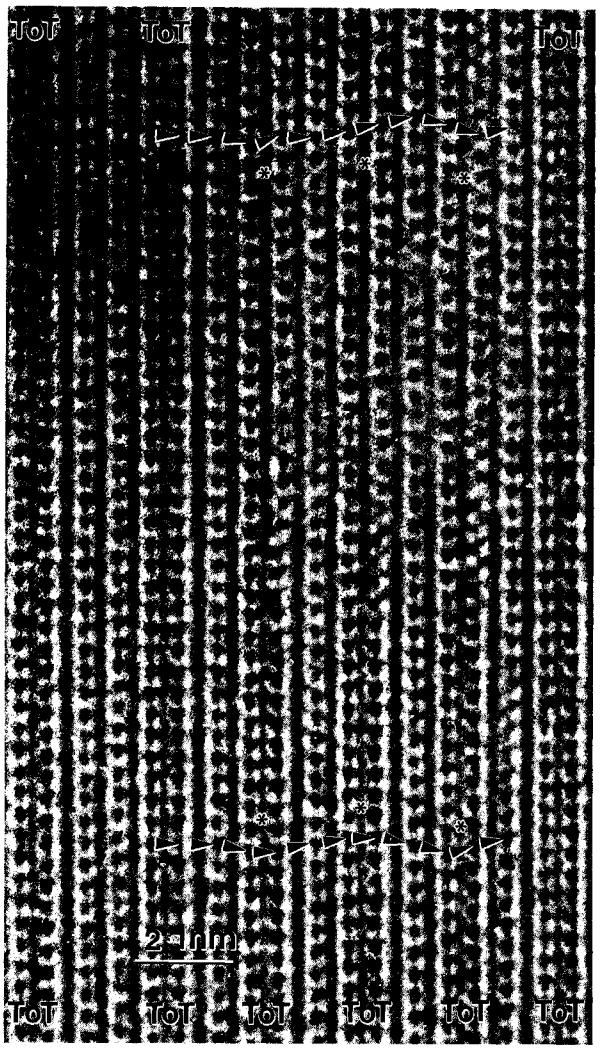

FIGURE 2. HRTEM structural image down [100] illustrating serpentine 1:1 layers (top center) passing smoothly into dozyite. Asterisks mark continuous layers in which the stacking sequences differ. Note that changes in stacking occur at the point of tetrahedral inversion, where two 1:1 layers pass into a chlorite unit.

ferent layer sequences are not uncommon (Fig. 3). Careful examination of image details reveals numerous areas where brucite-like interlayers pass smoothly into octahedral sheets of either 1:1 layers or 2:1 layers. The boundary zone between S_1C_1 sequences, such as defined by arrows at tetrahedral inversion points in Figure 3, is a region where layers are out of phase. Stacking order often varies across this boundary.

d_{001} = 2.8 nm. Although serpentine with a 2.8 nm periodicity in 20*l* is common (I,I,II,II and I,I,I,II; Banfield et al. 1995), the phase with a 2.8 nm 00*l* periodicity is extremely rare. Comparison of observed 00*l* intensities (Fig. 4) with those calculated for S_2C_1 (the only possible combination of 1.4 and 0.7 nm units producing a 2.8 nm 00*l* periodicity) uniquely identifies this phase. Extra pairs of serpentine layers are common in semirandomly interstratified serpentine-chlorite, and a few repeat S_2C_1 sequences are occasionally present in all S_xC_y phases (e.g., lower left side of Fig. 2).

d_{001} = 3.5 nm. Almost all SAED patterns with a 3.5 nm 00*l* period have strong 002, 003, and 005 reflections [i.e., a pair of strong reflections midway between the 00*l*, $l = 5n$ (subcell) reflections; Fig. 5c]. The distinctive pattern of 00*l* intensities can be simulated if the structure is S_1C_2 but not if it is S_3C_1 (Figs. 5a and 5b). The atomic resolution image showing the S_1C_2 sequence (Fig. 6a, but with one extra dozyite unit) verifies the structure inferred from the 00*l* intensity pattern. Note that the positions of tetrahedral cations inferred from the HRTEM image (Fig. 6a) and extensive streaking of 0*kl*, $k \neq 3n$ in the SAED pattern indicate stacking disorder, as found in the coexisting five-layer serpentine. In the [100] zone, the 3.5 nm periodicity is strong only in 00*l* (Fig. 6b), ruling out the possibility that it is an artifact introduced by dynamical diffraction. Beam damage is concentrated at the point where a 2:1 layer with an $a/3$ shift parallel to the beam direction passes into a 2:1 layer with an $a/3$ displacement along a pseudo-a axis (projected displacement of $b/3$; see arrows in Fig. 6a).

The 20*l* intensity pattern strongly resembles that of the 00*l* row (and the 20*l* intensity pattern from the intimately associated five-layer serpentine; see Fig. 2 in Banfield et al. 1995). There is no significant intensity in any 20*l* reflection other than the pair midway between the subcell maxima.

Intensities of 20*l* reflections were calculated for all possible octahedral sequences in both possible 3.5 nm phases, including all variants based on location of type-I and type-II octahedra in the 2:1, brucite-like, and 1:1 layers. SAED patterns for the I,I,I,I,I octahedral sequence have no kinematic intensity in the 20*l* row. However, when dynamical effects are incorporated, the 20*l* row intensities mimic those of the 00*l* row (especially apparent at specimen thicknesses > 4 nm). All other octahedral sequences produce intensities that are mixtures of 20*l* reflections derived from the octahedral sequence and dynamically induced reflections from the 00*l* row.

d_{001} = 4.2 nm. Minerals with a definite 4.2 nm 00*l* periodicity are extremely rare. All crystals were defective, and so no SAED patterns could be obtained from material entirely free of serpentine and chlorite impurities. The pattern shown in Figure 7c has a strong 1.4 nm reflection. If the relatively high intensity of this reflection is not entirely due to intergrown chlorite, comparison with the 00*l* intensities calculated for S_2C_2 and S_4C_1 would suggest the phase is S_2C_2. Because of the scarcity of crystals and the poor quality of their patterns, this identification must be regarded with caution.

d_{001} = 4.9 nm. Crystals with 4.9 nm 00*l* periodicities were encountered occasionally. Two patterns of 00*l* intensities were observed, indicating two different 4.9 nm phases. These periodicities could arise in four ways (S_5C_1, $S_1C_1S_2C_1$, S_3C_2, or S_1C_3). Each possible structure produces a distinct series of 00*l* intensities (Figs. 8a–8d). The

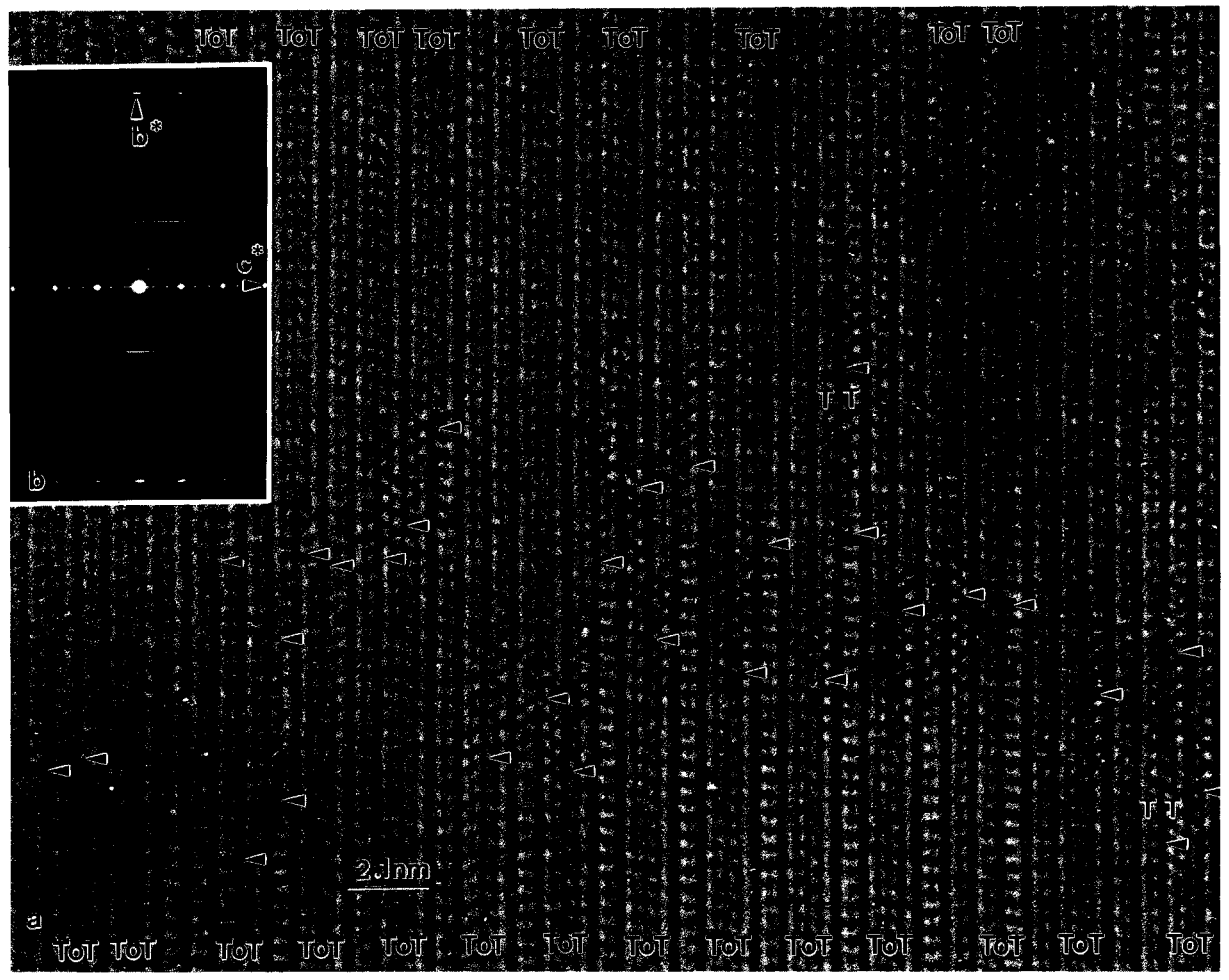

FIGURE 3. (a) HRTEM image showing the interface between S_1C_1 containing three S_2C_1 defects (bottom) and serpentine containing S_1C_1 and other sequences. Arrows indicate transition points (e.g., between S_2 and chlorite C_1). (b) SAED pattern showing the 2.1 nm 00*l* periodicity due to S_1C_1 (and 0.7 nm period due to serpentine). Textures suggest nucleation of chlorite at separate points in preexisting serpentine, with convergence creating out-of-phase interfaces.

first observed pattern (Fig. 8e) can be interpreted to arise from S_3C_2, whereas the second (more common) pattern (Fig. 8f) can be attributed to S_1C_3. The latter identification is verified by examination of the atomic resolution image in Figure 9. In the [100] zone, the 4.9 nm period is present only in 00*l*, and the 0*kl*, $k \neq 3n$ reflections are continuously streaked (Fig. 9b) indicating stacking disorder. Arguments regarding the octahedral cation sequences as inferred from the intensity of 20*l* reflections for the 3.5 nm phase apply to the 4.9 nm phases, indicating I,I,I,I,I,I,I sequences in both cases.

d_{001} = 6.3 nm. SAED patterns from the [100] and [010] zones of the 6.3 nm phase are shown in Figures 10a and 10b. The characteristic pair of maxima midway between the 0.7 nm 00*l* reflections is simulated in Figure 10c, confirming the structure of this phase as S_1C_4. Streaking of 0*kl*, $k \neq 3n$ indicates semirandom stacking.

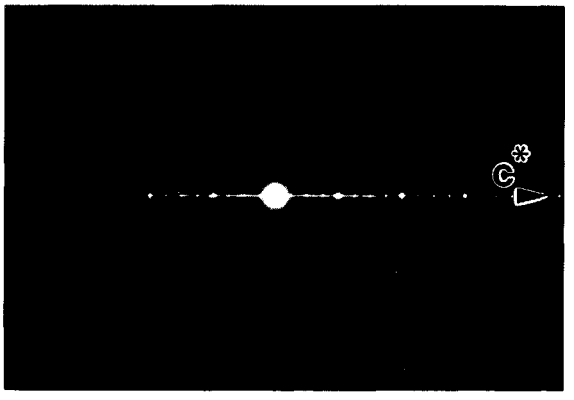

FIGURE 4. SAED pattern showing a 2.8 nm periodicity in 00*l*. Because no reflections other than the 00*l* reflections were in a diffracting condition, the periodicity cannot be explained by dynamical diffraction (e.g., involving the 20*l*s of four-layer serpentine) and must be due to the S_2C_1 phase.

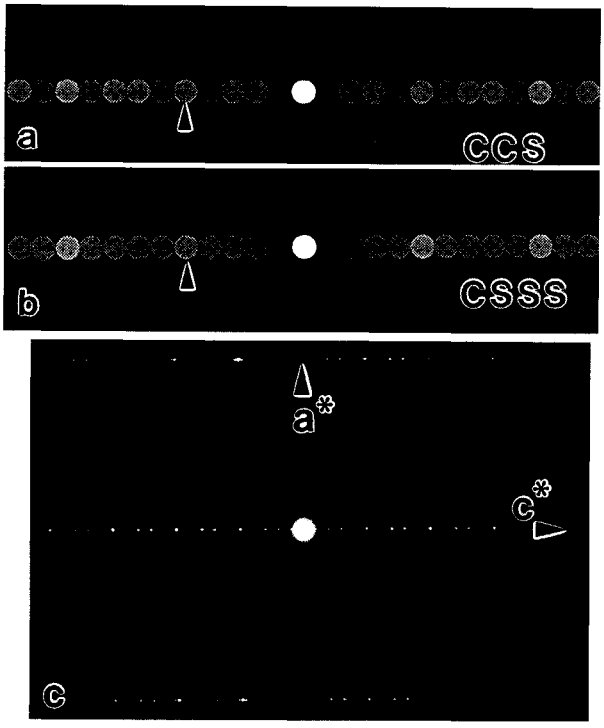

FIGURE 5. Calculated 00*l* intensities for S_1C_2 (**a**) and S_3C_1 (**b**). Intensities in **a** match those observed in the [010] SAED pattern from the phase with 3.5 nm periodicities in 00*l* and 20*l* in **c** as well as 00*l* intensities (Fig. 6b). Those calculated for S_3C_1 do not match. Arrows in **a** and **b** mark the 0.7 nm substructure reflection common to all patterns.

Chlorite

Chlorite is a minor constituent of the assemblage. Intensity distributions in 20*l* reflections and the magnitudes of the β angles indicate the presence of the I*bb* and, in a very small percentage of cases, the II*bb* polytype. Some SAED patterns with 2.8 nm 20*l* and, occasionally, 02*l* periodicities suggest the presence of some two-layer chlorite. Chlorite stacking is almost always semirandom. Most crystals contain defects consisting of extra 1:1 layers.

To test further the extent to which 20*l* reflections from chlorite can be interpreted to provide structural information, we prepared a sample of a well-characterized II*bb* chlorite previously described by Zheng and Bailey (1989). SAED patterns displayed clear intensity variations that could be used to identify the polytype.

Relative abundances of layer silicates

The predominant minerals in the serpentine are serpentine and randomly interstratified serpentine-chlorite. Overall, the order of abundance is serpentine > random interstratifications > S_1C_1 > chlorite (primarily I*bb*) > S_1C_2 > S_1C_3 > S_1C_4 ≫ S_2C_2 > S_2C_1, etc. Although four- and six-layer serpentines are relatively common, regular interstratifications that contain more serpentine than chlorite (e.g., S_2C_1) are rare. The strong predominance of chlorite-rich over serpentine-rich regular interstratifications, despite the abundance of appropriate serpentine precursors, supports the view that the prograde serpentine-to-chlorite reaction favors S_1C_1 and more chlorite-rich polysomes.

Discussion

Interpretation of HRTEM images (on the basis of comparisons with image simulations) and 00*l* intensities in SAED patterns (on the basis of comparisons with patterns calculated for all possible layer sequences with the appropriate *c*-axis periodicities) revealed that the serpentinite contains six minerals based on the regular interstratification of serpentine and chlorite (Table 3). Analysis of positions and intensities of 0*kl* and 20*l* reflections in SAED patterns revealed these minerals and chlorite have $\beta = 90°$ and semirandom stacking, and contain octahedra with a single tilt. Of these, only dozyite (S_1C_1; Bailey et al. 1995) and S_2C_1 (Banfield et al. 1994) have been previously described in detail. Unlike the sample described by Banfield et al. (1994) and Bailey et al. (1995) that contained dozyite [I*aa*-(2,4,6); $\beta = 94.4°$] and serpentine-rich regular interstratifications, the regular interstratification assemblage reported here is dominated by dozyite ($\beta = 90°$; I*bbb*,I) and minerals based primarily on combinations of a single serpentine with different numbers of chlorite units.

Dozyite, longer period regular interstratifications, and chlorite are characterized by a single octahedral cation type, whereas the serpentine assemblage is dominated by group-D standard polytypes and longer period serpentines characterized by complex sequences of type-I and type-II octahedra. Within the precision of the AEM technique, all layer silicates have the same composition. Thus, most layer silicates in the assemblage are metastable, their existence reflects kinetic rather than thermodynamic factors.

On the basis of geological evidence, it is probable that chlorite and random and regular interstratifications of serpentine-chlorite formed from serpentine. Furthermore, because the mechanism involved direct structural transformation (see below), minerals containing a single 1:1 layer surrounded by multiple chlorite units could not have formed from chlorite without substantial structural reconfiguration of surrounding chlorites.

What sort of long-range interactions operated over sufficiently large distances that they could control the development of sequences of structural units with repeats up to 6.3 nm? Normal coulombic interactions are unlikely to allow structural communication over such large scales. If long-period regular interstratifications form by a solid-state mechanism, the answer may lie in the structural details of the coexisting minerals.

Banfield et al. (1995) suggested that long-period serpentine polytype formation occurred during the extreme deformation event that resulted in the macroscopic preferred orientation in all layer silicates in serpentine samples. Polytype formation may have involved layer-parallel shear or periodic twinning during recovery, as

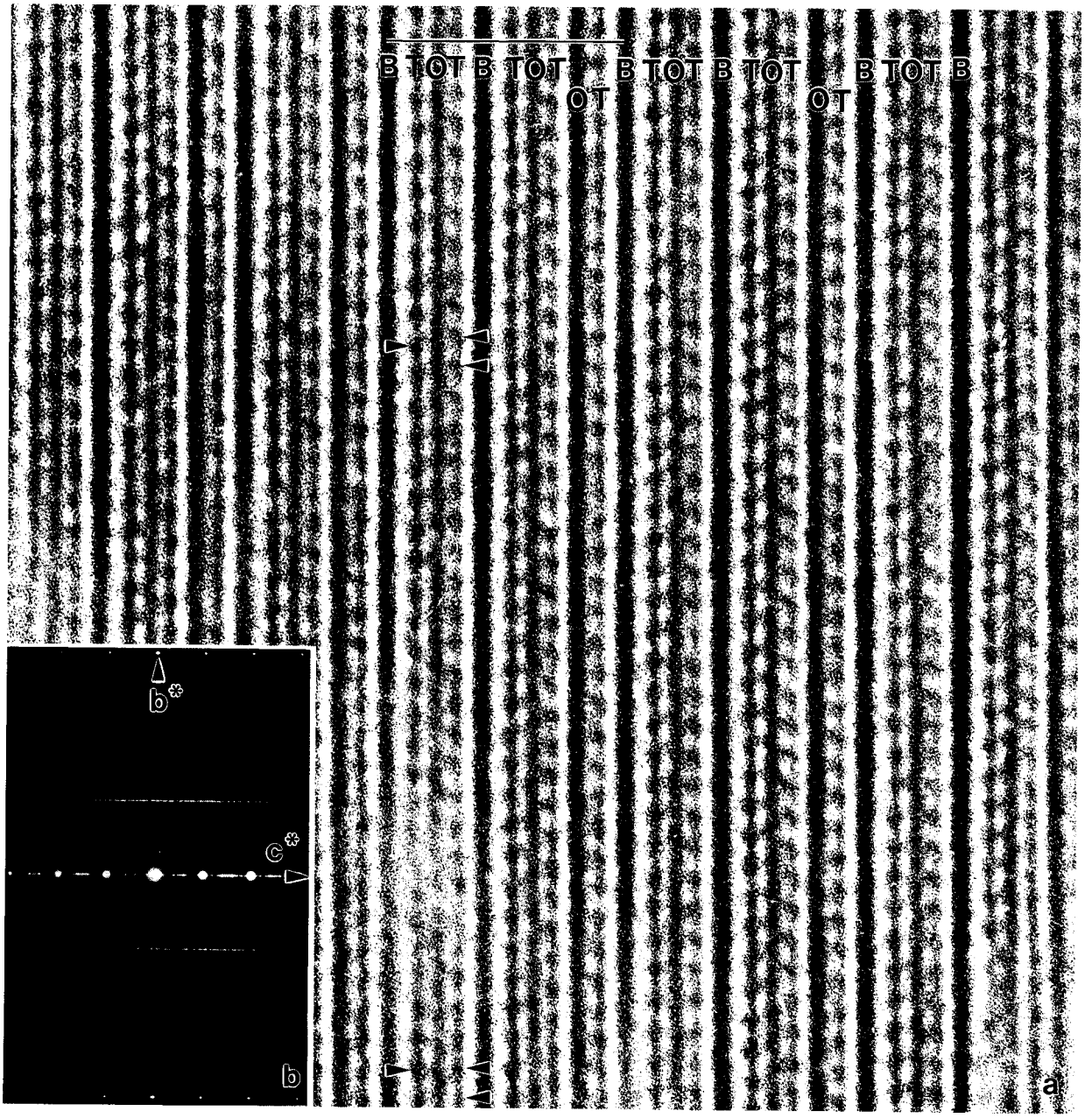

FIGURE 6. (**a**) HRTEM structural image down [100] illustrating an area composed primarily of regularly interstratified S_1C_2. A dozyite defect is present to the left of the single arrows. Electron-beam damage is focused where a 2:1 layer with $+b/3$ shift passes into a layer with zero shift (see arrows). (**b**) SAED pattern for **a** illustrating a 3.5 nm periodicity in $00l$ and intensities similar to those shown in Figure 5b. Note the continuous streaking of $0kl$, $k \neq 3n$, indicating no true periodicity for basal O atoms along c^* (semirandom stacking).

suggested by Banfield et al. (1995), or spiral growth on screw dislocations, as proposed by Baronnet and coworkers for micas (e.g., Baronnet 1975). Regardless of how this complex assemblage of serpentine polytypes formed, their coexistence with the S_xC_y phases leads us to suggest that formation of the regular interstratifications is the direct consequence of the preexistence of the long-period serpentines.

We propose that periodicities in the long-period serpentines are inherited by S_xC_y phases and that serpentine octahedral sequences dictate the serpentine-chlorite sequence in the S_xC_y. Because interactions between adjacent 1:1 layers differ, depending upon whether adjacent layers have the same or different octahedral tilts, I,II sequences may be more unstable than I,I sequences (or vice versa). Thus, changes in metamorphic conditions (e.g.,

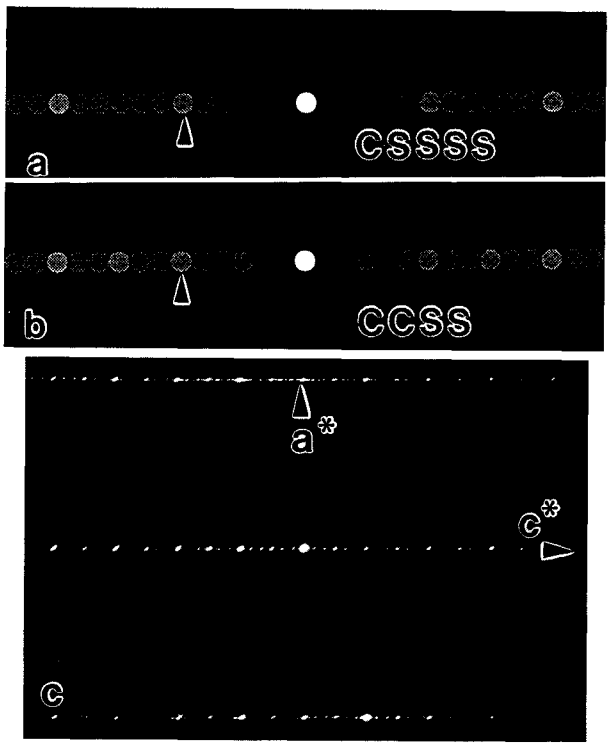

FIGURE 7. Calculated 00*l* intensities for S_4C_1 (**a**) and S_2C_2 (**b**). Intensities in the [010] SAED pattern from the 4.2 nm phase (**c**) match those in **b** if the strong 00*l* reflection midway between the subcell reflections is not due to intergrown chlorite.

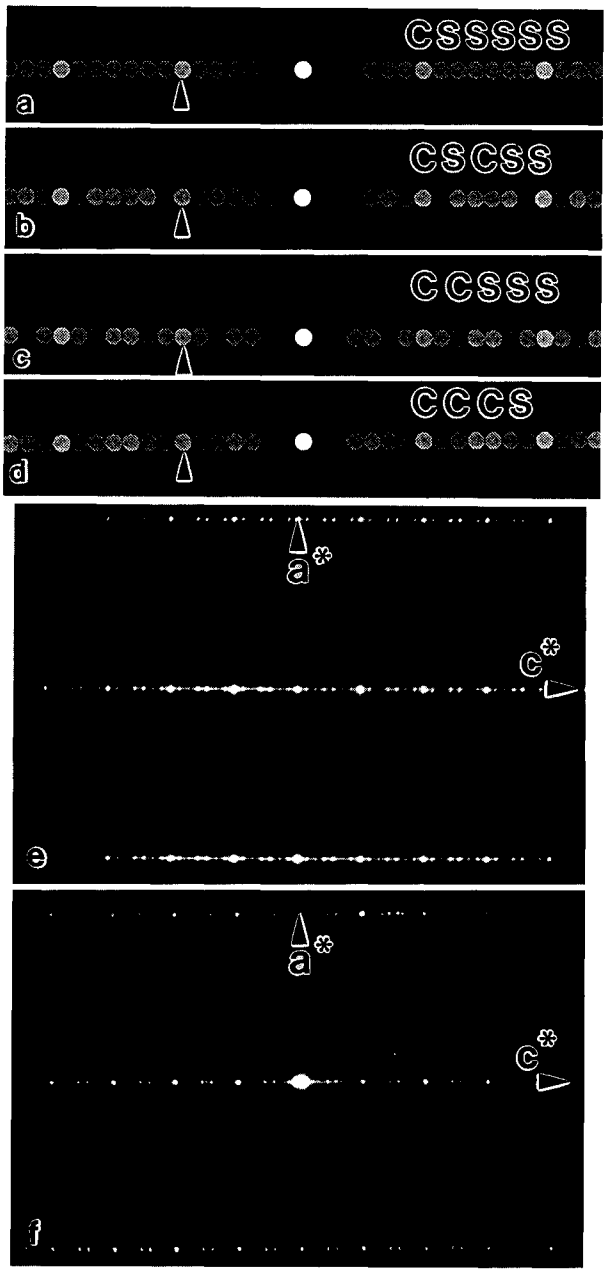

FIGURE 8. Calculated 00*l* intensities for a mineral with a 4.9 nm periodicity due to regular interstratification of (**a**) S_5C_1, (**b**) $S_2C_1S_1C_1$, (**c**) S_3C_2, (**d**) S_1C_3. The 00*l* intensities in the [010] SAED pattern in **e** match S_3C_2, and those in **f** match S_1C_3.

pressure) might destabilize specific layer pairs, resulting in their selective replacement by chlorite. For example, if I,II sequences are destabilized preferentially in a I,I,I,II serpentine, the product would be S_2C_1. These hypotheses can be tested because they place important constraints on structural characteristics of the minerals involved. First, appropriate long-period serpentine polytypes should exist and their distributions should correlate with those of the long-period regular interstratifications. Furthermore, the number and position of chlorite units in each S_xC_y structure should be consistent with the number and distribution of pairs of 1:1 layers with either I,I or I,II sequences in coexisting long-period serpentines. Second, the stacking (sequence of *b*/3 displacements) and octahedral cation sequence should be either inherited from serpentine or modified in a way consistent with the reaction mechanism.

All observations are consistent with the formation of regular and randomly interstratified serpentine-chlorite by direct replacement of a preexisting layer silicate. Interfaces between serpentine and chlorite are regions where serpentine octahedral sheets pass smoothly into brucite-like sheets or the octahedral sheet of 2:1 layers, or are inherited directly by the 1:1 serpentine unit in the regular interstratifications (Fig. 2). Out-of-phase relationships (e.g., Fig. 3) are interpreted to result from convergence of chlorite units that nucleated at different points in a serpentine crystal.

Out-of-phase phenomena are consistent with the above hypothesis, which specifies only that sub-sequences (e.g., I,II) in long-period serpentines are converted to chlorite. For example, S_1C_1 could form from a three-layer sequence (. . . I,I,II,I,I,II . . .) in one of two ways. Reading from the left, the first I,II sequence could become the chlorite. Alternatively, the first II,I sequence could convert to chlorite. If both possibilities occurred in the same

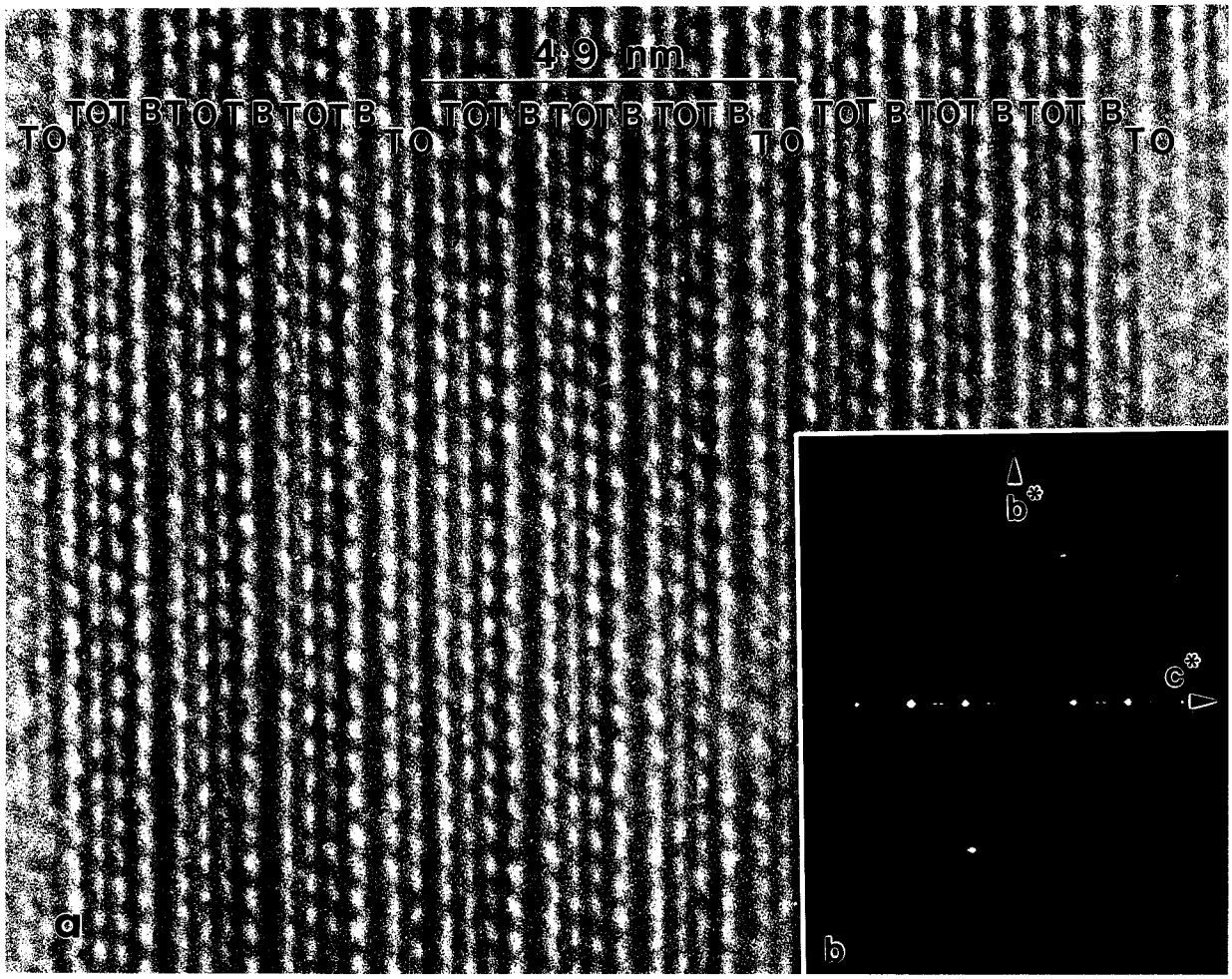

FIGURE 9. (a) HRTEM structural image down [100] illustrating an area of regularly interstratified S_1C_3. The SAED pattern in b shows the 4.9 nm 00*l* periodicity with the intensity distribution shown in Figures 8d and 8f. Stacking disorder is apparent.

TABLE 3. Comparison between abundances and structures of long-period serpentine polytypes and regularly interstratified serpentine-chlorite minerals

Serpentine*			S_xC_y		
Period (nm)	Octahedral structure	Abundance	Structure**		Abundance
2.1	II,I,I	abundant	S_1C_1	I*bbb*,I	relatively abundant
2.8	I,II,II,I	relatively abundant	? C_2	(chlorite)	rare
2.8	II,I,I,I	relatively abundant	S_2C_1	I*bbb*,I	extremely rare
3.5	I,II,I,II,I	moderately abundant	S_1C_2	I*bbb*,I	moderately abundant
4.2	I,II,II,I,I,I	moderately abundant	? S_2C_2		extremely rare
4.9	I,II,I,II,I,II,II	occasional	S_1C_3	I*bbb*,I	occasional
4.9	II,I,II,I,I,I,I	rare	S_3C_2	I*bbb*,I	rare
6.3	Not determined	rare	S_1C_4		rare

Note: Underlines emphasize the correlation between the number and distribution of I,II sequences in serpentines and chlorite units in regular interstratifications.

* From Banfield et al. (1995).

** Terminology of Banfield et al. (1994).

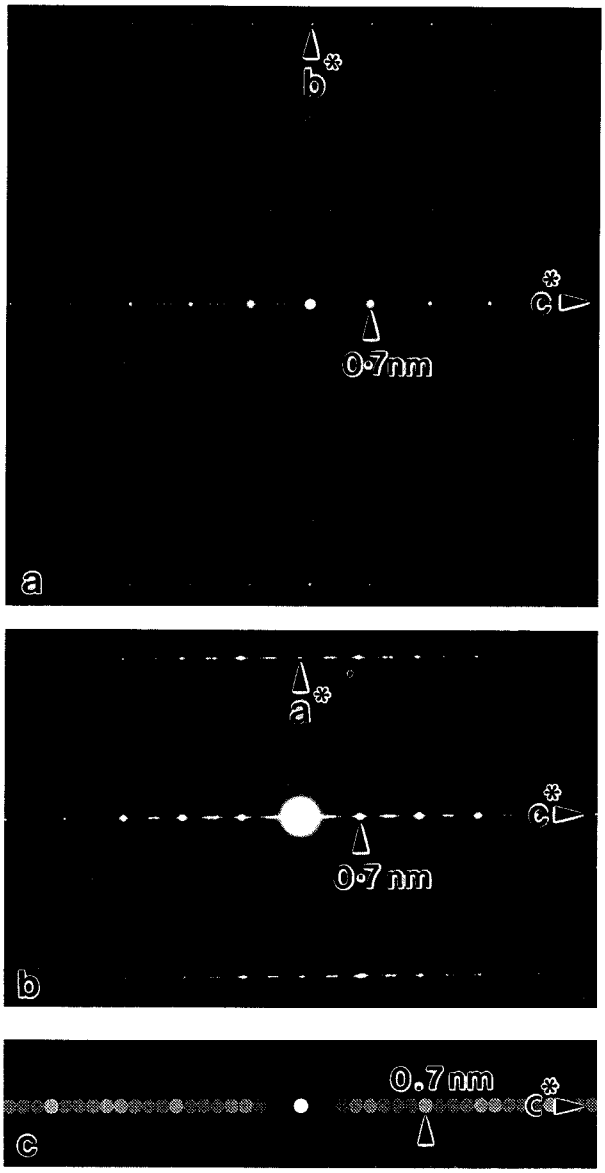

FIGURE 10. (a) The [100] and (b) [010] SAED patterns of the 6.3 nm phase that is based on regular interstratification (S_1C_4). (c) Calculated intensities for S_1C_4, which match 00*l* intensities in **a** and **b**.

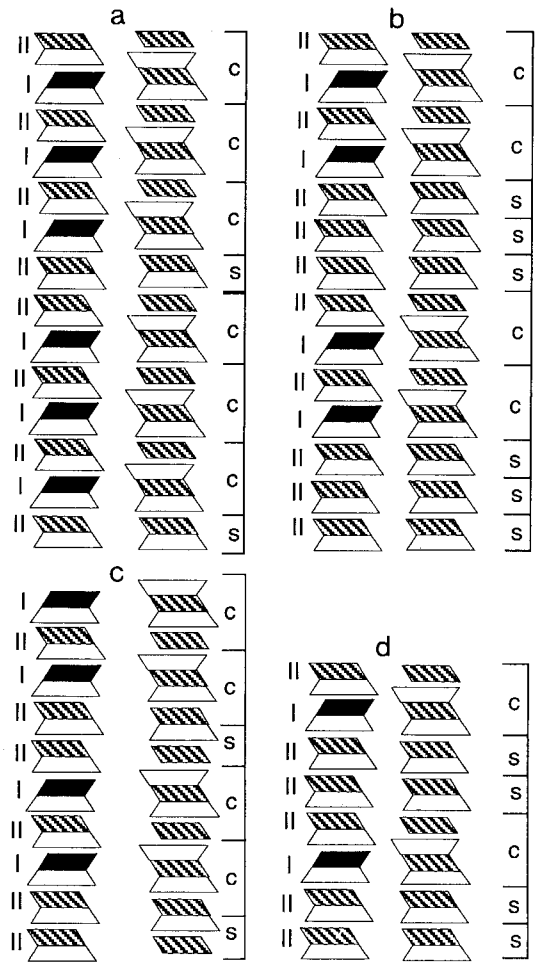

FIGURE 11. Schematic diagram down [010] showing four examples where selective replacement of pairs of 1:1 layers (S) with I,II octahedral slants in long-period polytypes [(**a**) II,I,II,I,II,I,II; (**b**) II,II,II,I,II,I,II; (**c**) II,II,I,II,I; (**d**) II,II,I,II] by chlorite (C) leads to regular interstratifications with the sequences of chlorite and serpentine units known to occur in the assemblage [(**a**) S_1C_3; (**b**) S_3C_2; (**c**) S_1C_2; (**d**) S_2C_1]. The same result is achieved for the 2.1 nm serpentine (I,I,II) and S_1C_1 (see Fig. 13). Octahedral sequences of serpentines in the assemblage are from Banfield et al. (1995). Note that formation of the 2:1 layers must involve conversion of type-II to type-I octahedra to produce regular interstratifications characterized by a single octahedral tilt.

crystal, the chlorite layers would be out of register at the interface between the two regions.

For each S_xC_y mineral there exists a serpentine with the same *c*-axis periodicity (random stacking), and the distributions of long-period serpentines and long-period regular interstratifications with equal *c*-axis periodicities are generally correlated. Table 3 shows a pattern involving correspondence between the number of I,II sequences in serpentine (underlined; Banfield et al. 1995) and the number and position of chlorite units in S_xC_y. This suggests that the periodicity of the regular interstratification is determined by the *c*-axis periodicity of the precursor serpentine and that the positions of chlorite units in S_xC_y are determined by preferential replacement of pairs of 1:1 layers with I,II octahedral tilts.

Why should I,II sequences be converted selectively to chlorite? Because polytypes differ in their octahedral tilt sequences they almost certainly have different structural energies and should exhibit differential stability. The structural energy of a I,I sequence differs from that of a I,II sequence because octahedral Mg cations project directly onto Mg cations in the adjacent 1:1 layer in the I,I sequence but not in the I,II sequence. The magnitude of this effect is probably small because interactions that distinguish these structures operate over distances of 0.7 nm.

Although the connection between these cationic interactions and thermodynamic stability is unclear, a difference in stability must exist, and this lends support to the concept that formation of regular interstratifications may be caused by replacement of octahedral cation sub-sequences.

If regular interstratifications form from preexisting serpentines with long-period octahedral cation sequences, the octahedral cation sequence in the regular interstratification should be the same as in the serpentine, at least in parts of the structure that are unmodified by the reaction. Our data show that all octahedra are type I in the regular interstratifications, unlike octahedra in associated serpentines. If all type-II octahedra are converted to type I as a consequence of replacement of pairs of 1:1 layers with I,II octahedral tilts by 2:1 layers and a brucite-like interlayer, resulting interstratifications would be characterized by a single octahedral tilt (Fig. 11).

Evidence for restructuring at the juncture between continuous 1:1 and 2:1 layers is found in HRTEM images, which show that the sequence of zero or projected $b/6$ displacements is always modified by formation of a chlorite unit (e.g., see arrows in Fig. 2). Changes are localized within the 2:1 layer that forms when the T-O connectivity is modified (Figs. 2 and 3). As noted above, the intralayer vector of $a/3$ along the a or pseudo-a axes is seen in [100] images as a zero or projected $b/6$ displacement (see Fig. 5, Bailey et al. 1995).

Regions where chlorite units pass continuously into two 1:1 layers could form during growth. However, the fact that random sequences of $b/3$ displacements between layers in serpentine at the top and dozyite at the bottom of Figure 2 are common to both dozyite and serpentine (except where the interlayer shift becomes the intralayer displacement in the 2:1 layer) provides very strong evidence that one phase formed from the other. It should be noted that the basic concept of essentially solid-state interconversion of serpentine and chlorite is not new (e.g., Brindley and Gillery 1954; Baronnet 1992). The validity of this hypothesis is strengthened by observations reported here.

The first steps in the formation of chlorite from lizardite probably include protonation of an apical O, rupture of the Si-O bond, and repositioning of Si below the basal O plane. In general, most common serpentines belong to groups C and D. These serpentines are characterized by zero or $\pm b/3$ stacking vectors (groups A and B have $a/3$ interlayer stacking vectors and are apparently quite unstable because of interaction between octahedral and tetrahedral cations in adjacent layers; Brown and Bailey 1962; Shirozu and Bailey 1965). For groups C and D, and related long-period serpentines, Figure 12 shows that tetrahedral inversion does not place the Si in a tetrahedral coordination environment. Furthermore, O atoms that form the top surface of the 2:1 layer are not positioned correctly to form hydrogen bonds with the new brucite-like interlayer. Thus, displacement of Si and its coordinating bridging O is required. Hydrogen bonding requires that the Si and O shift be $\pm a/3$. As shown in Figure 13, a shift of $+a/3$ avoids superposition of the overlying octahedral cation in the brucite-like interlayer on the Si (the type-b arrangement; Brown and Bailey 1962). (For a 2:1 layer growing left-to-right, this shift is required for space reasons.) The alternative $-a/3$ shift would result in the energetically unfavorable superposition of tetrahedral and octahedral cations (type-a interaction; Brown and Bailey 1962), producing a II*ab* sequence. To our knowledge, II*ab* chlorite has never been reported. Furthermore, ~89% of known chlorite structures completely avoid type-a interactions (Bailey 1988a, 1988b). These observations testify to the energetic disadvantage of the type-a configuration.

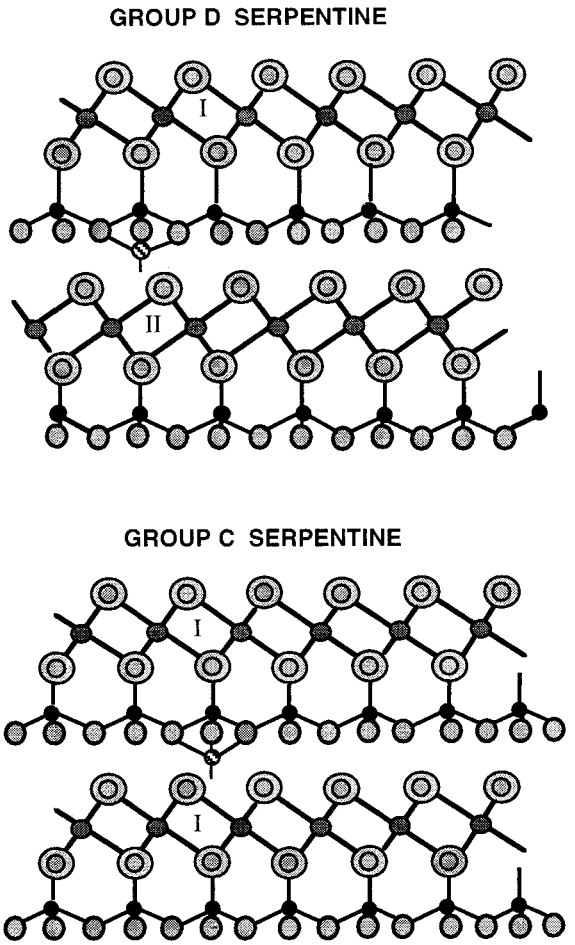

FIGURE 12. Diagram down [010] showing that for group-D and group-C serpentine (only zero and $\pm b/3$ shifts), tetrahedral inversion places Si in a position where it cannot achieve coordination with an apical O without translation. Locally, long-period serpentine polytypes in the assemblage have either group-C or group-D characteristics.

The $+a/3$ shift in Figure 13 ($-a/3$ shift in the case where octahedral slants in the 1:1 layers are reversed) requires repositioning of octahedral cations in the new 2:1 layer from type-II to type-I sites. Thus, the change in octahedral tilt upon formation of the 2:1 layer (Fig. 11) follows as a consequence of structural inversion, explaining the I,I, . . .

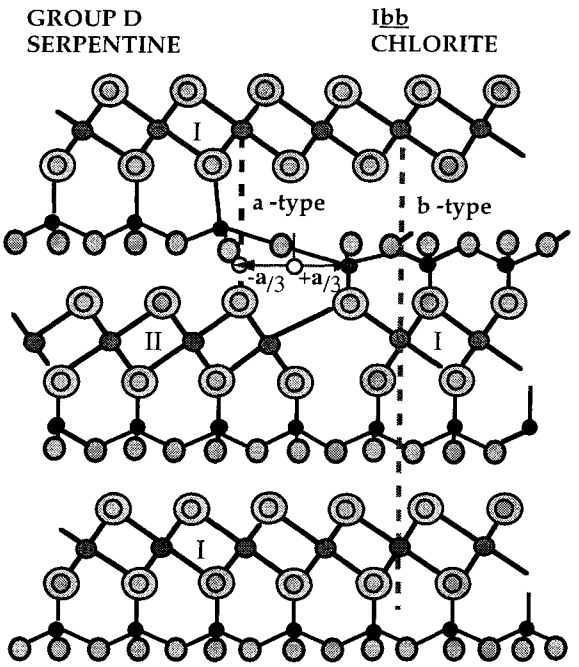

FIGURE 13. Diagram down [010] showing the results of $+a/3$ and $-a/3$ Si shifts needed for hydrogen bonding after tetrahedral inversion. This shift is imaged directly in Figure 2. A $-a/3$ shift would preserve the octahedra of the 2:1 layer but would result in energetically unfavorable superposition of octahedral and tetrahedral cations (type-a interaction), as shown by the dashed line on the left side of the diagram. A $+a/3$ shift avoids this superposition (type-b interaction), as shown by the dashed line on the right side of the diagram. The $+a/3$ shift necessitates movement of octahedral cations in the 2:1 layer, converting the octahedra from type II to type I. If tetrahedral inversion occurs in any pair of 1:1 layers with opposing tilts, the result is generally a chlorite in which the octahedral tilts are identical. In detail, the $a/3$ shift results in considerable distortion of the tetrahedra at the end of the inverting 1:1 layer. This may lower the activation barrier for inversion of the next tetrahedra.

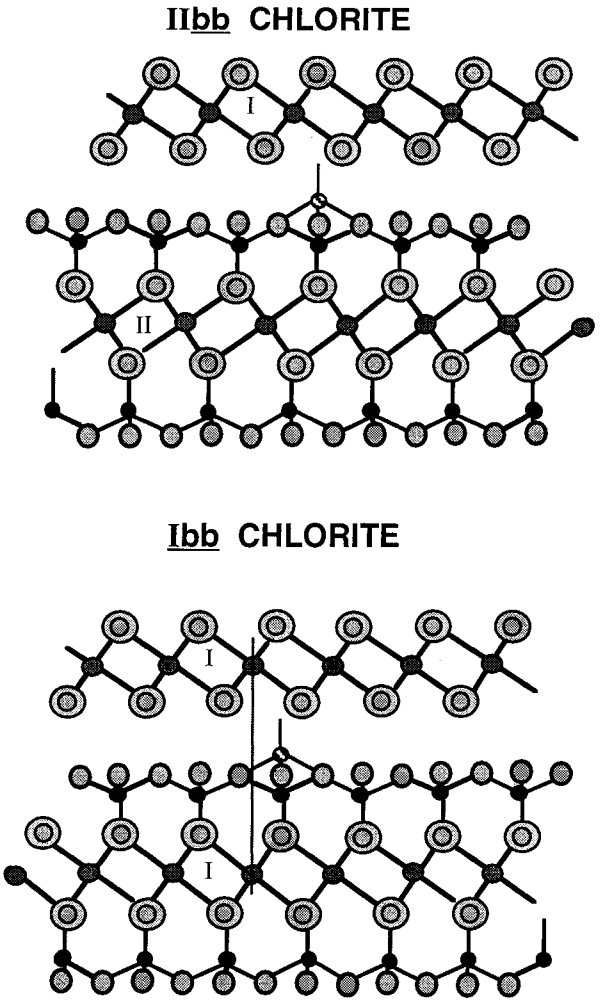

FIGURE 14. Diagram down [010] showing that if conversion of the common II*bb* and less common I*bb* chlorite polytypes to serpentine occurs by tetrahedral inversion, tetrahedral cations and associated O atoms must shift parallel to a to achieve an appropriate coordination environment and hydrogen bonding. In the case of inversion in II*bb* chlorite, the argument regarding type-a vs. type-b interactions given for Figure 13 may result in production of lizardite-1*T*. For I*bb* chlorite, lizardite-1*T* can be produced by translation of Si and basal O without restructuring the octahedral portion of the new 1:1 layer.

sequence in all regular interstratifications as well as the imaged projected $a/3$ shift in Figures 2 and 3.

In addition to change of apical Si-O bond lengths in the inverted portion (to adjust the thickness of the 2:1 layer), H must diffuse from the upper surface of the 1:1 layer to the brucite-like interlayer. The timing of H diffusion and the possible role of additional H, OH, or H_2O are not known (although the transformation may be isochemical and is essentially isovolumetric, these components may catalyze the reaction). Rupture of the apical (nonbridging Si-O) bond in the inverting tetrahedra and relocation of Si below the O plane may be facilitated by tetrahedral distortion, allowing Si to reposition without rupture of its bonds to basal O atoms. The activation energy for rupture of the apical Si-O bond may be lowered because the Si-O bonds in the tetrahedra linked to the inverted portion are elongated (Fig. 13) and thus weakened. Therefore, "zippering" of the 2:1 layer proceeds once growth of the 2:1 layer commences.

In summary, serpentines with long-period octahedral cation sequences and stacking disorder formed in the serpentine, possibly as the result of deformation. Subsequent metamorphism induced conversion of serpentine to chlorite. This occurred by direct structural transformation, with inheritance of all structural characteristics of layers not involved in tetrahedral inversion. Chlorite formed preferentially from pairs of 1:1 layers with differing oc-

tahedral slants. Type-II octahedra were converted to type-I octahedra because the 2:1 layer formed by tetrahedral inversion in directly superimposed layers, and the required shifts of the tetrahedral elements were controlled by the need for hydrogen bonding and minimization of cationic interactions.

An interesting characteristic of the assemblage of regularly interstratified serpentine-chlorite minerals is the extreme rarity of 2.8 and 4.2 nm phases and the complete absence of a 5.6 nm phase. The low abundance of regular interstratifications of 2.8 nm cannot be explained by scarcity of appropriate serpentine precursors. These observations support the suggestion that prograde serpentine-to-chlorite reactions produce S_1C_1 and more chlorite-rich phases and that retrograde reactions produce S_1C_1 and serpentine-rich structures (Banfield et al. 1994).

Chlorite-to-serpentine reactions are common under retrograde metamorphic conditions. The pathway for this reaction is probably controlled by the chlorite structure. Commonly, the reaction involves the II*bb* polytype, in which the brucite-like interlayer has a slant that differs from that of the octahedral sheet of the 2:1 layer. Walker (1993) reported only two occurrences of I*bb* chlorite out of 47 occurrences of chlorite in altered igneous rocks. (The reason why all but two of tens of crystals from the Woods serpentine were I*bb* is not known.) Figure 14 illustrates that tetrahedral inversion in both II*bb* and I*bb* chlorites results in a situation analogous to that described above for the serpentine-to-chlorite reaction. Given the inferred, large energetic cost of a-type interactions, it is possible to speculate that both I*bb* and II*bb* chlorites convert to the very common lizardite-1*T* structure.

Inconsistency between stacking in 1*T* lizardite and the inversion product of II*bb* chlorite was pointed out by Baronnet (1992). However, our data suggest that the requirement for relocation of anions and cations in layers involved in tetrahedral inversion does not preclude a solid-state reaction.

This is the second paper describing in detail the structures and distributions of members of a serpentine-chlorite polysomatic series. Our findings are supplemented by those of Xu and Veblen (1993) and by the unpublished data of Kominou and Veblen (Veblen 1993 personal communication) and of Livi and Veblen (Livi 1993 personal communication), which indicate that these minerals may be common in serpentine- and chlorite-bearing rocks. The existence of S_xC_y phases may have been overlooked because they are less abundant constituents of chlorite- and serpentine-dominated assemblages. Although these phases contribute additional peaks to XRD powder diffraction patterns, low abundances in complex layer-silicate mixtures probably make their characteristic peaks easy to overlook. However, results presented here demonstrate that, if the S_xC_y phases are sufficiently abundant, it should be possible to identify layer sequences using relative 00*l* intensities in XRD powder patterns from oriented mounts.

Acknowledgments

We thank R.C. Smith for samples and W.W. Barker for assistance in sample preparation and discussion. This paper was improved by the comments of Ken Livi and Huifang Xu. This research was partially supported by NSF grants EAR-9317082 and EAR-9117386 to J.F.B. and a grant from the Department of Geology and Geophysics, University of Wisconsin, to S.W.B.

References cited

Bailey, S.W., Ed. (1988a) Hydrous phyllosilicates exclusive of micas, 725 p. Mineralogical Society of America, Washington, DC.

Bailey, S.W. (1988b) X-ray identification of the polytypes of mica, serpentine, and chlorite. Clays and Clay Minerals, 36, 193–213.

Bailey, S.W., Banfield, J.F., and Barker, W.W. (1993) Regular interstratifications of serpentine/chlorite, p. 11. Proceedings of the 10th ICC, Adelaide, Australia.

Bailey, S.W., and Banfield, J.F. (1995) Derivation and identification of nonstandard serpentine polytypes. American Mineralogist, 80, 1104–1115.

Bailey, S.W., Banfield, J.F., Barker, W.W., and Katchan, G. (1995) Dozyite, a 1:1 regular interstratification of serpentine and chlorite. American Mineralogist, 80, 65–77.

Banfield, J.F., Bailey, S.W., and Barker, W.W. (1993) Polysomatism, polytypism, microstructures and reaction textures in serpentine and chlorite. Clay Minerals Society Meeting Program and Abstracts, p. 86.

Banfield, J.F., Bailey, S.W., and Barker, W.W. (1994) Polysomatism, polytypism, microstructures and reaction mechanisms in serpentine and chlorite. Contributions to Mineralogy and Petrology, 117, 137–150.

Banfield, J.F., Bailey, S.W., Barker, W.W., and Smith, R.C., II (1995) Complex polytypism: Relationships between serpentine structural characteristics and deformation. American Mineralogist, 80, 1116–1131.

Baronnet, A. (1975) Growth spirals and complex polytypism in micas: I. Polytype structure generation. Acta Crystallographica, A31, 345–355.

——— (1992) Polytypism and stacking disorder. In Mineralogical Society of America Reviews in Mineralogy, 27, 231–282.

Brindley, G.W., and Gillery, F.M. (1954) Mixed-layer kaolin-chlorite. Clays and Clay Minerals, 2nd National Conference, 349–353.

Brown, B.E., and Bailey, S.W. (1962) Chlorite polytypism: I. Regular and semi-random one-layer structures. American Mineralogist, 47, 819–850.

Lapham, D.M. (1958) Preliminary report on the chromite occurrence at the Wood Mine, Pennsylvania. Pennsylvania Geological Survey Progress Report 153, 11 p.

Reynolds, R.C. (1988) Mixed layer chlorite minerals. In Mineralogical Society of America Reviews in Mineralogy, 19, 601–628.

Reynolds, R.C., and Hower, J. (1970) The nature of mixed-layer illite-montmorillonite. Clays and Clay Minerals, 18, 25–36.

Shirozu, H., and Bailey, S.W. (1965) Chlorite polytypism: III. Crystal structure of an orthohexagonal iron chlorite. American Mineralogist, 50, 868–885.

Stadelmann, P. (1991) Simulation of HREM images and 2D CBED patterns using EMS software package. Software manual 12M-EPFL, Lausanne, Switzerland.

Thompson, G.R., and Hower, J. (1975) The mineralogy of glauconite. Clays and Clay Minerals, 23, 289–300.

Walker, J.R. (1993) Chlorite polytype geothermometry. Clays and Clay Minerals, 41, 260–267.

Xu, H., and Veblen, D.R. (1993) Periodic and disordered interstratification and other microstructures in the chlorite-berthierine series. Geological Society of America Program and Abstracts, A-146.

Zheng, H., and Bailey, S.W. (1989) Structures of intergrown triclinic and monoclinic II*b* chlorites from Kenya. Clays and Clay Minerals, 37, 308–316.

Manuscript received November 11, 1994
Manuscript accepted September 26, 1995